# Dynamic quasicrystalline patterns: Wave-mode–Turing-mode resonance with Turing-mode self-interaction

Ziad H. Musslimani
*Department of Mathematics, Technion–Israel Institute of Technology, Technion City, 32000 Haifa, Israel*

Len M. Pismen
*Department of Chemical Engineering and Minerva Center for Nonlinear Physics of Complex Systems, Technion–Israel Institute of Technology, Technion City, 32000 Haifa, Israel*

(Received 19 August 1999; revised manuscript received 13 March 2000)

We study perturbatively the effect of resonant Turing-mode interactions on the slow time evolution of quasicrystalline patterns sustained by resonant interaction between wave and static composite modes. We find that stabilization of quasicrystalline patterns by quadratic wave-mode–Turing-mode interactions is possible even under the action of weak *destabilizing* Turing-mode self-interactions.

PACS number(s): 05.45.−a, 42.65.Sf

## I. INTRODUCTION

A quasicrystalline pattern is a fascinating but rather elusive form of *complex order*. Constructing such patterns may seem easy: in two dimensions they can be formed just by superposing four or more noncollinear modes [1]. Near a symmetry-breaking transition from a homogeneous to a patterned or crystalline state (in both equilibrium and nonequilibrium systems) these modes appear formally as degenerate neutrally stable eigenmodes of linearized macroscopic equations, and may admit, in various contexts, different physical interpretations, e.g., density waves in equilibrium theory [2]. In practice, however, it has turned out rather difficult to find conditions that allow selection of a quasicrystalline pattern by nonlinear interactions. A possible source of quasicrystalline patterns is a superposition of two resonant triplets of Turing modes [3]. This pattern can be stabilized, however, only by quadratic interactions, which strongly inhibit multimode patterns, since interaction between the modes directed at small angles tends to be mutually damping. Quasicrystalline patterns of Turing type were, however, observed in experiments with parametric excitation of surface waves (Faraday instability) [4,5]. Conditions suitable for formation of quasicrystalline Turing patterns were detected by the analysis of model equations [6] as well as of the amplitude equations of the Faraday instability [7]. Patterns formed by two resonant triplets were shown to be one of the possible states of Marangoni convection in a layer with a deformable interface [8]. A sure recipe for creating a quasicrystal is *rotation* of the optical field in a nonlinear cavity [9–14]. The number of modes is dictated then by the rotation angle. If it is commensurate with $2\pi$, so that $\Delta = 2\pi n/N$ (where $n$ and $N$ are integers that do not have common factors), the basic planform is a rotationally invariant combination of $N$ or $N/2$ plane waves (respectively, for $N$ odd or even), which yields a quasicrystalline pattern at $N = 5, 7,$ or more.

Recently, Pismen and Rubinstein [14–16] suggested resonant interaction among Turing modes and wave modes near a degenerate bifurcation point as a powerful mechanism of formation of quasicrystalline patterns. Patterns involving resonant interactions are likely to exhibit complex dynamics of amplitude modulation on a slow time scale due to intermittent phase locking. It has indeed been shown that resonant quasicrystalline patterns often appear as *dynamic* patterns with ever changing appearance but a permanent composition of the Fourier spectrum. A degenerate bifurcation of modes with different wavelengths can be arranged most readily in nonlinear optical systems, as demonstrated in experiments by Arrecchi and co-workers [12,13], as well as theoretical and modeling studies [14–19]. An interesting feature of the wave-mode–Turing-mode resonance is the possibility of preventing unlimited growth of the amplitudes by the action of quadratic (three-wave) interactions only. The small-amplitude solutions in the vicinity of this degenerate bifurcation can be either stationary, periodic, or chaotic [16]. The analysis of Pismen and Rubinstein did not include resonant three-wave interactions between Turing modes, however, which generically leads to a subcritical bifurcation to a hexagonal pattern. These interactions are always *destabilizing*, so that nonuniversal (and generically weaker) cubic (four-wave) interaction has to be introduced in order to prevent the runaway.

The question we shall investigate here is whether stabilization by quadratic wave-mode–Turing-mode interactions only is possible also when interactions between Turing modes are present. The set of amplitude equations including interactions between Turing modes, which will be formulated in Sec. II and analyzed in Sec. III, turns out to be substantially more complicated than a system lacking these interactions, due to the presence of an additional dynamic phase. We shall show in the Appendix that the required conditions for wave-mode–Turing-mode resonance can be achieved in a three-component reaction-diffusion system that is much simpler than nonlinear optical systems considered in earlier studies.

We shall see in Sec. III that the stability region of stationary states is reduced but not eliminated when Turing-mode self-interactions are present. Oscillatory states will be studied in Sec. IV in the limit of weak Turing-mode–Turing-mode coupling when a modified scaling can be applied to obtain a stable limit cycle at intermediate amplitudes.

 

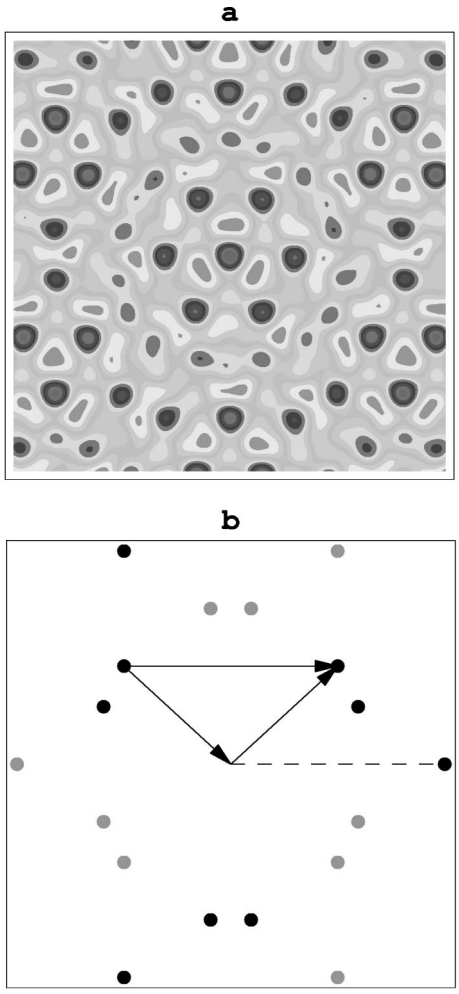


FIG. 1. The planform (2.2) with $N=3$ (nine modes). A snapshot of a real space (near field) pattern (a) and the corresponding structure in Fourier space (far field) (b). The inner (outer) circles correspond to wave (Turing) modes. Complex conjugate modes are denoted by gray circles. One of the wave-mode–Turing-mode resonant triangles is shown, and the participating Turing mode is indicated by the dashed line.

## II. AMPLITUDE EQUATIONS

Our starting point is a set of amplitude equations in the vicinity of a degenerate wave-mode–Turing-mode bifurcation. We suppose that the underlying system (homogeneous and isotropic in two space dimensions) possesses a codimension-2 bifurcation manifold where a Turing and a wave mode are neutrally stable, and consider a point on this manifold where the wave numbers of the Turing and wave modes are, respectively, $Q$ and $k$. The directions of the corresponding wave vectors are arbitrary, and the number of excited modes cannot be determined *a priori*.

The amplitude equations are obtained using the standard methods of bifurcation expansion in a dummy small parameter $\epsilon$. In the leading order, the amplitudes of the excited modes, the deviation from the bifurcation manifold, and the inverse slow time scale of the amplitude evolution are all of $O(\epsilon)$. The amplitude equation of some mode (denoted, say, by the index zero) contains a quadratic term contributed by interactions between two other modes (indexed, say, 1 and 2) if and only if the wave vectors $\boldsymbol{k}_i$ and frequencies $\omega_i$ of the three modes satisfy the resonance conditions

$$\boldsymbol{k}_1+\boldsymbol{k}_2=\boldsymbol{k}_0, \quad \omega_1+\omega_2=\omega_0. \tag{2.1}$$

A resonant triplet may involve therefore either three static (Turing) modes ($\omega=0$) with wave vectors at the angle $\pi/3$ or two wave modes with identical frequencies $\omega_i$ and one static mode. In the latter case, the vertex angle of the isosceles resonant triangle depends on the ratio of wave numbers of the Turing and wave modes, which must not exceed 2. A possible first-order resonant structure is built of $N$ Turing modes with the amplitudes $a_j$ and $2N$ wave modes with the amplitudes $b_j$ and $c_j$:

$$\boldsymbol{u}_1=\mathrm{Re}\sum_{j=1}^{N}\{a_j\boldsymbol{V}_s\exp(i\boldsymbol{Q}_j\cdot\boldsymbol{r})+e^{i\omega t_0}[b_j\exp(i\boldsymbol{q}_j\cdot\boldsymbol{r}) + c_j\exp(i\boldsymbol{k}_j\cdot\boldsymbol{r})]\boldsymbol{V}_w\}, \tag{2.2}$$

where $\boldsymbol{V}_s$ and $\boldsymbol{V}_w$ are the eigenvectors corresponding to the Turing and Hopf modes, respectively, and the resonance condition $\boldsymbol{q}_j-\boldsymbol{k}_j=\boldsymbol{Q}_j$ is satisfied. The validity of Eq. (2.2) is a nontrivial issue, i.e., if the wave vectors do not lie on a regular lattice then at high orders wave vectors arbitrarily close to the neutral curve can be excited. However, the problem of high-order wave vectors close to the neutral curve is important for *stationary* quasipatterns but not for oscillatory patterns, since even in the case where the high-order wave vectors are close to the neutral curve, the corresponding high-order frequency is very high and strongly different from $\omega$. The minimal structure including also Turing-mode–Turing-mode resonance is obtained at $N=3$. An example of a quasicrystalline planform (transverse pattern) corresponding to such a nine-mode structure is shown in Fig. 1. The lowest-order amplitude equations including all possible triplet interactions are

$$\begin{aligned}\dot{a}_j&=-\mu_s a_j+\lambda_s a_{j+1}^* a_{j-1}^*+\nu_s b_j c_j^*,\\ \dot{b}_j&=\mu_w b_j+\nu_w a_j c_j,\\ \dot{c}_j&=\mu_w c_j+\nu_w a_j^* b_j.\end{aligned} \tag{2.3}$$

We exclude nongeneric cases when the angle between the wave modes in the resonant triangle is a multiple of $\pi/6$. All the coefficients appearing in the above amplitude equations can be expressed through the parameters of the underlying problem under study. The coefficients $\mu_s$ and $\mu_w$ depend on the deviation from the bifurcation manifold, while $\nu_s$, $\nu_w$, and $\lambda_s$ are computed at the bifurcation point itself; $\mu_s$, $\nu_s$, and $\lambda_s$ are real, while $\mu_w$ and $\nu_w$ are complex. A dynamical system similar to Eq. (2.3) but lacking the Turing-mode self-interaction term (i.e., with $\lambda_s=0$) has been obtained for optical cavities with rotated beam [14], a two-component feedback optical system [15], and an optical cavity with sodium vapor in a magnetic field [19]. In the Appendix we analyze a simpler example of a three-component reaction-diffusion system and apply the method of multiple-scale bifurcation expansion to derive Eqs. (2.3).

### III. SMALL-AMPLITUDE DYNAMICS

In what follows, we shall study the influence of the Turing-mode–Turing-mode interaction on the dynamics of the resonant transverse patterns. We assume that the complex amplitudes of the three static modes are equal, and those of the wave modes fall into two groups of three equal amplitudes. When only resonant Turing modes are present, the equal-amplitude planform is typically chosen in the vicinity of the bifurcation manifold, while higher-order interactions are still negligible, which leads to a common hexagonal pattern [20]. The system (2.3), generally, does not possess gradient structure and cannot be assigned energy (Lyapunov functional). Nevertheless, the choice of an equal-amplitude state is natural, and is necessary to make the problem tractable. Further on, this requirement will be relaxed by requiring only the moduli, but not the phases, of the amplitudes to be equal.

The system (2.3) reduces now to three complex equations which can be further reduced to five real equations for real amplitudes and phases using the polar representation of the complex amplitudes,

$$a_j=\rho_a e^{i\theta_a},\quad b_j=\rho_b e^{i\theta_b},\quad c_j=\rho_c e^{i\theta_c}. \tag{3.1}$$

The relevant variables are the three real amplitudes $\rho_j$ and the composite phases $\theta=\theta_a+\theta_c-\theta_b$ and $\phi=3\theta_a$. The amplitude equations can be further rescaled to a form containing three real parameters only. The imaginary part of $\mu_w$ can be absorbed in the frequency, and three more real parameters are eliminated by rescaling the amplitudes and time. It can be shown that the condition $\mu_s>0$ is necessary to prevent runaway to large amplitudes (which may be further arrested by third- and higher-order terms). Assuming this condition holds, we rescale time by $\mu_s$ and denote $\mu=\mu_w/\mu_s$. The resulting equations are

$$\begin{aligned}
\dot{\rho}_a&=-\rho_a+\rho_b\rho_c\cos\theta+\kappa\rho_a^2\cos\phi,\\
\dot{\rho}_b&=\mu\rho_b+\rho_a\rho_c\cos(\theta-\alpha),\\
\dot{\rho}_c&=\mu\rho_c+\rho_a\rho_b\cos(\theta+\alpha),\\
\dot{\theta}&=-\rho_b\rho_c\rho_a^{-1}\sin\theta-\rho_a\rho_b\rho_c^{-1}\sin(\theta+\alpha)\\
&\quad-\rho_a\rho_c\rho_b^{-1}\sin(\theta-\alpha)-\kappa\rho_a\sin\phi,\\
\dot{\phi}&=-3\kappa\rho_a\sin\phi-3\rho_b\rho_c\rho_a^{-1}\sin\theta,
\end{aligned} \tag{3.2}$$

where we have set $\nu_w=|\nu_w|e^{-i\alpha}$; $\kappa=\lambda_s/|\nu_w|$ and $|\nu_w|$, $\nu_s$ have been absorbed by rescaling the amplitudes. In what follows, we reiterate the case with $\kappa=0$. In this case, the equation for $\phi$ decouples. The remaining system of four equations admits a stationary symmetric solution (with equal wave amplitudes)

$$\theta=0,\quad \rho_a=-\mu/\cos\alpha,\quad \rho_b=\rho_c=\sqrt{-\mu/\cos\alpha}, \tag{3.3}$$

and a stationary asymmetric solution with different wave amplitudes and $\theta=\theta_0$, where

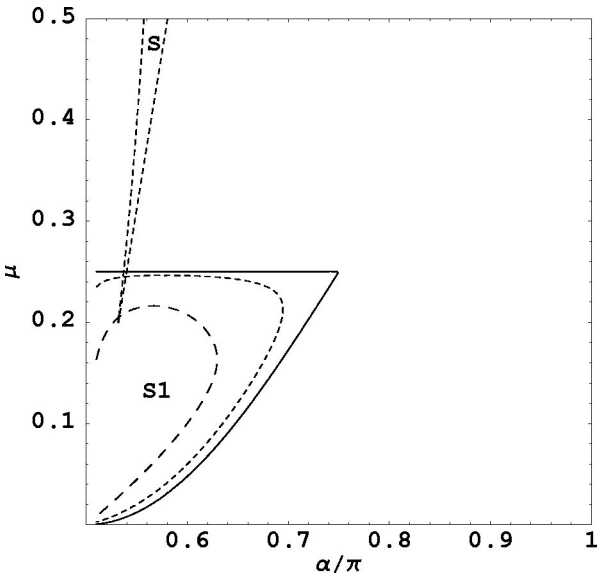


FIG. 2. Bifurcation diagram of Eq. (3.2) in the $(\mu,\alpha)$ parameter space for $\mu>0$ and $\cos\alpha<0$. Letters $S1$ and $S$ denote the regions of stable stationary symmetric solutions with $\theta=\phi=0$ and $\theta=\pi,\phi=0$, respectively. In $S1$, the solid line corresponds to $\kappa=0$, the dotted line to $\kappa=0.01$, and the dashed line to $\kappa=0.1$. In the $S$ region, the dashed line corresponds to $\kappa=0.5$.

$$\cos^2\theta_0=\sin^2\alpha/(1+2\mu). \tag{3.4}$$

In the symmetric case, $\phi$ is an arbitrary constant. This degeneracy corresponds to the translational symmetry of the pattern. On the other hand, the asymmetric solution generates a dynamic state of the full five-dimensional system with $\phi=\phi_0-\Omega t$ where $\Omega=3\rho_b\rho_c\sin\theta_0/\rho_a$.

The stability of the symmetric and asymmetric states has been analyzed in [15], where a bifurcation diagram in the $(\mu,\alpha)$ parametric plane was constructed. In various parametric domains, the system may relax to either a symmetric or an asymmetric stationary state, to a periodic orbit that corresponds to slow modulation of the basic pattern on an extended time scale of Eq. (2.3), or to a chaotic attractor on the same extended scale. For $\kappa\neq0$, the degeneracy of the symmetric solution is broken, and $\phi$ has to be fixed in the stationary state at either 0 or $\pi$; it is easy to see that only solutions with $\phi=0$ are stable. This gives rise to two stationary symmetric solutions. One of them,

$$\theta=0;\quad \rho_a=-\mu/\cos\alpha,\quad \rho_b=\rho_c=\sqrt{\rho_a(1-\kappa\rho_a)}, \tag{3.5}$$

reduces to Eq. (3.3) at $\kappa\to0$. On the contrary, the second solution,

$$\theta=\pi,\quad \rho_a=-\mu/\cos\alpha,\quad \rho_b=\rho_c=\sqrt{\rho_a(\kappa\rho_a-1)}, \tag{3.6}$$

is subject to the conditions $\mu\cos\alpha<0$, $\rho_a>1/\kappa$ and disappears at $\kappa\leqslant\kappa_c=-\cos\alpha/\mu$, so that it has no counterpart in the absence of Turing-mode–Turing-mode interaction.

Applying the Routh-Hurwitz stability criterion, one can obtain the stability boundaries of both states. The numerical results for different values of $\kappa$ are shown in Fig. 2. The stability region of the state $\theta=0$ retreats as $\kappa$ increases in the

interior of the stability region of the symmetric solution at $\kappa=0$. The two stability boundaries at $\kappa=0$, which correspond to the Hopf (straight line in Fig. 2) and pitchfork bifurcations (solid curve in the same figure), turn at $\kappa\neq 0$ into a single smooth curve, which corresponds to the Hopf bifurcation over its entire length. For the state $\theta=\pi$, which does not exist at $\kappa=0$, the stability region is smaller than the previous one, and shrinks on increasing $\kappa$ until it disappears at $\kappa\approx 0.8$. The region outside the stability boundaries may in general include periodic and chaotic dynamic states. One of such states (at $\kappa\ll 1$) is a perturbation of the above mentioned asymmetric dynamic solution.

## IV. INTERMEDIATE-AMPLITUDE DYNAMICS

We have seen that any nonzero value of $\kappa$, however small, introduces a singular perturbation that causes a qualitative change of the character of behavior, adding a new family of solutions which goes to zero and disappears at $\kappa \leqslant \kappa_c$. In the following, we shall concentrate upon dynamics at $\kappa\ll 1$, and apply the powerful technique of multiple-scale analysis to elucidate the dynamics of the magnified amplitudes. To ensure consistent scaling, we shall assume that, as $\kappa\ll 1$, the real part of $\nu_w$ is of $O(\kappa)$ and write $\nu_w=-\kappa\nu+i\eta$; thus, we restrict ourselves to the case $\cos\alpha=O(\kappa)$ (cf. Fig. 2). The real amplitudes on the new branch of solutions diverge at $\kappa\to 0$ with different powers; thus we have to rescale the amplitudes $a_j$, $b_j$, and $c_j$ as $a_j=A_j/\kappa$, $b_j=B_j/\sqrt{\kappa}$, and $c_j=C_j/\sqrt{\kappa}$. Recalling that the amplitude equations describe small-amplitude dynamics, $a,b=O(\epsilon)$, we have to require that $\kappa$, though small, satisfy the inequality $\epsilon\ll\kappa$. We shall therefore consider the dynamics at ''intermediate'' amplitudes. The rescaled Eq. (2.3) takes the form

$$\begin{aligned}\dot{A}_j&=-A_j+A^*_{j+1}A^*_{j-1}+B_jC^*_j,\\ \dot{B}_j&=\mu B_j-(\nu-i\eta/\kappa)A_jC_j,\\ \dot{C}_j&=\mu C_j-(\nu-i\eta/\kappa)A^*_jB_j.\end{aligned}\tag{4.1}$$

Notice that at $\kappa\ll 1$ and, respectively, $\cos\alpha\approx-\kappa\nu$, the solutions (3.5) and (3.6) have the same scaling as $A_j,B_j,C_j$ and, indeed, are stationary solutions of Eq. (4.1). When rewritten in the rescaled variables, Eq. (3.5) becomes $|A|=\mu/\nu$, and

$$|B|=|C|=\sqrt{|A|(1-|A|)},\quad \arg(AC/B)=0,\tag{4.2}$$

while the solution (3.6) takes the form

$$|B|=|C|=\sqrt{|A|(|A|-1)},\quad \arg(AC/B)=\pi.\tag{4.3}$$

Next, we apply the multiple-scale perturbation expansions and introduce a hierarchy of time scales,

$$\partial/\partial t=\kappa^{-1}\partial/\partial\tau_0+\partial/\partial\tau_1\cdots,$$

and then expand the amplitude $\boldsymbol{A}_j\equiv(A_j,B_j,C_j)$ in a Taylor series in $\kappa$:

$$\boldsymbol{A}_j=\boldsymbol{A}^0_j+\kappa\boldsymbol{A}^1_j+\ldots.$$

Using the above expansions in the system (4.1), we find in the leading order $O(\kappa^{-1})$ that the Turing amplitudes $A^0_j$ depend on the slow time scale $\tau_1$ only. The zero-order equations are

$$\begin{aligned}\frac{\partial A^0_j}{\partial\tau_1}&=-\frac{\partial A^1_j}{\partial\tau_0}-A^0_j+A^{0*}_{j+1}A^{0*}_{j-1}+B^0_jC^{0}*,\\ \frac{\partial B^0_j}{\partial\tau_0}&=i\eta A^0_jC^0_j,\quad \frac{\partial C^0_j}{\partial\tau_0}=i\eta A^{0}*B^0_j.\end{aligned}\tag{4.4}$$

The solution to the last two equations of the system (4.4) is given by

$$\begin{aligned}B^0_j&=B^+_j(\tau_1)e^{i\eta\zeta}+B^-_j(\tau_1)e^{-i\eta\zeta},\\ C^0_j&=C^+_j(\tau_1)e^{i\eta\zeta}+C^-_j(\tau_1)e^{-i\eta\zeta},\end{aligned}\tag{4.5}$$

where $B^+_j=C^+_je^{i\varphi_j}$, $B^-_j=-C^-_je^{i\varphi_j}$, and we define $\zeta\equiv\rho_0\tau_0$ and $A^0_j=\rho_0e^{i\varphi_j}$.

To obtain evolution on the slow scale, we define the linear operator $\hat{\mathcal{F}}_j=\partial^2/\partial\tau_0^2+\eta^2|A^0_j|^2$. Then the first-order equations are written as

$$\begin{aligned}\hat{\mathcal{F}}_jB^1_j&=\partial\mathcal{S}_j/\partial\tau_0+i\eta A^0_j\mathcal{T}_j,\\ \hat{\mathcal{F}}_jC^1_j&=\partial\mathcal{T}_j/\partial\tau_0+i\eta A^{0*}_j\mathcal{S}_j,\end{aligned}\tag{4.6}$$

where $\mathcal{S}_j$ and $\mathcal{T}_j$ are defined by

$$\begin{aligned}\mathcal{S}_j&=-\partial B^0_j/\partial\tau_1+\mu B^0_j-\nu A^0_jC^0_j+i\eta C^0_jA^1_j,\\ \mathcal{T}_j&=-\partial C^0_j/\partial\tau_1+\mu C^0_j-\nu A^{0*}_jB^0_j+i\eta B^0_jA^{1*}_j.\end{aligned}\tag{4.7}$$

We assume that the moduli of the amplitudes of all static modes are equal and those of wave modes fall into two groups of three equal moduli. In contrast with the preceding section, we make this assumption regarding moduli only, while the phases of all modes are allowed to be different. Averaging the first equation in the system (4.4) over the fast time scale yields

$$\begin{aligned}\frac{\partial A^0_j}{\partial\tau_1}&=-A^0_j+A^{0*}_{j+1}A^{0*}_{j-1}+\langle B^0_jC^{0*}_j\rangle_{\tau_0},\\ \frac{\partial A^1_j}{\partial\tau_0}&=B^0_jC^{0}*-\langle B^0_jC^{0*}_j\rangle_{\tau_0},\end{aligned}\tag{4.8}$$

where the average over the fast time scale is defined by

$$\langle F\rangle_{\tau_0}=\lim_{T\to\infty}\frac{1}{T}\int_0^T F(\tau_0)d\tau_0.\tag{4.9}$$

Substituting the solution (4.5) into the first equation of the system (4.8) and computing the average, we find

$$\dot{\rho}_0 = -\rho_0 + \rho_0^2 \cos\varphi + |B_j^+|^2 - |B_j^-|^2,$$
$$\dot{\varphi} = -3\rho_0 \sin\varphi, \tag{4.10}$$

where the overdot denotes the time derivative with respect to $\tau_1$, and $\varphi = \varphi_1 + \varphi_2 + \varphi_3$. It is clear that the total phase always relaxes to zero, while the phases of the wave modes do not affect the evolution of the Turing mode. To derive the dynamic equations for the slowly varying amplitudes $B_j^{\pm}$, one has to substitute the solution (4.5) into the second equation of (4.8) and integrate it to obtain $A_j^1$. Next, we substitute $A_j^1$ and Eq. (4.5) in Eq. (4.6) and eliminate secular terms contributed by the real part of the right hand side of the system (4.6). In polar representation, $B_j^{\pm} = \rho_{\pm} e^{i\theta_j^{\pm}}$, the equations take the form

$$\dot{\rho}_0 = -\rho_0 + \rho_0^2 + \rho_+^2 - \rho_-^2,$$
$$\dot{\rho}_+ = \left(\mu + \frac{\rho_-^2}{2\rho_0} - \nu\rho_0\right)\rho_+, \tag{4.11}$$
$$\dot{\rho}_- = \left(\mu - \frac{\rho_+^2}{2\rho_0} + \nu\rho_0\right)\rho_-.$$

The equation for the phases $\theta_j^{\pm}$ is similar to the equation of $\varphi$; thus, all phases decay to zero, and are irrelevant. Thus, we find that the three complex equations (2.3) are reduced to three real amplitude equations. Next, we investigate the dynamics of the above system. To prevent runaway to infinity (which might be further arrested by adding higher-order terms), we exclude the case $\mu > 0$, $\nu < 0$. The fixed points of the system (4.11) correspond to *periodic orbits* of Eq. (4.1). The stationary solution with all three amplitudes differing from zero is

$$\rho_0 = 1 - 4\mu, \quad \rho_{\pm} = \sqrt{2\rho_0(\nu\rho_0 \pm \mu)}, \tag{4.12}$$

subject to the conditions $-\nu\rho_0 < \mu < \nu\rho_0$. Applying the Routh-Hurwitz stability criterion we find that this stationary solution is linearly unstable for *any* $\mu$ and $\nu$. Other stationary solutions of Eq. (4.11) lie on the invariant manifolds $\rho_+ = 0$ and $\rho_- = 0$, which we denote as $\mathcal{M}^{\pm}$, respectively. On $\mathcal{M}^-$ the reduced dynamics is given by

$$\dot{\rho}_0 = -\rho_0 + \rho_0^2 + \rho_+^2,$$
$$\dot{\rho}_+ = (\mu - \nu\rho_0)\rho_+. \tag{4.13}$$

The nontrivial fixed point is given by $\rho_0 = \mu/\nu$ and $\rho_+ = \sqrt{\rho_0(1-\rho_0)}$. For the positiveness of the amplitude we require $\mu\nu > 0$ and $\rho_0 < 1$. Linearizing system (4.13) about the above stationary solution shows that it is stable if $\nu > 0$ and $0 < \mu < \nu/2$. The stability of the invariant manifold $\mathcal{M}^-$ requires $\mu < \nu/(1+4\nu)$. Both stability conditions are shown in Fig. 3.

The bifurcation line $\nu = 2\mu$, shown by the dashed line in Fig. 3, corresponds to a degenerate *vertical* Hopf bifurcation [21]. Above this line, all trajectories run away to infinity. For

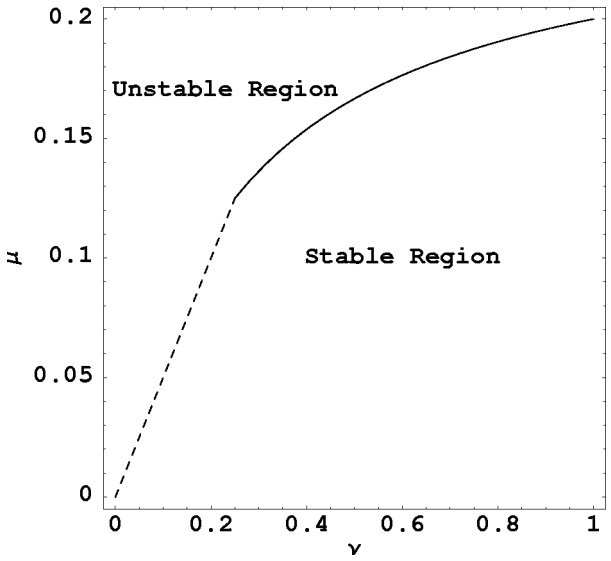


FIG. 3. Stability boundaries of the fixed point in the $(\mu, \nu)$ parameter space. The dashed line corresponds to a Hopf instability and the solid line to excitations on the invariant manifold $\mathcal{M}^-$.

each point on the line $\nu = 2\mu$, we find analytically a continuous family of periodic orbits, which correspond to *tori* of Eqs. (4.1). Indeed, rewriting the system (4.13) as a single ordinary differential equation,

$$\frac{d\rho_+}{d\rho_0} = \frac{\mu(1-2\rho_0)\rho_+}{\rho_+^2 + \rho_0^2 - \rho_0}, \tag{4.14}$$

and integrating Eq. (4.14) yields

$$[(1+2\mu)(\rho_0 - \rho_0^2) - \rho_+^2]\rho_+^{1/\mu} = \mathcal{E}, \tag{4.15}$$

where $0 \leqslant \mathcal{E} \leqslant \mathcal{E}_{\max} \equiv 2^{-(\mu+1)/\mu}\mu$. The largest closed trajectory corresponding to $\mathcal{E} = 0$ consists of the parabolic segment

$$\rho_+^2 = (1+2\mu)(\rho_0 - \rho_0^2), \quad \rho_0 > 0, \tag{4.16}$$

and the axis $\rho_0 = 0$. The orbits with $\mathcal{E} > 0$ lie within this orbit (see Fig. 4). All orbits are neutrally stable with respect to perturbations restricted to the invariant manifold $\mathcal{M}^-$. The stability of the periodic orbits with respect to perturbations orthogonal to the invariant manifold $\mathcal{M}^-$ is checked by integrating the last equation in the system (4.11):

$$\rho_-(\tau_1) = \rho_-(0)\exp\left(\int_0^{\tau_1} \Gamma(\rho_0(\xi), \rho_+(\xi))d\xi\right), \tag{4.17}$$

where we define

$$\Gamma(\rho_0, \rho_+) = \mu - \frac{\rho_+^2}{2\rho_0} + 2\mu\rho_0. \tag{4.18}$$

The periodic orbits are stable if

$$\int_0^T \Gamma(\rho_0(\tau_1), \rho_+(\tau_1))d\tau_1 < 0, \tag{4.19}$$

with $T = T(\mu)$ being the period of the oscillations. In what follows, we provide a sufficient condition for the trajectories

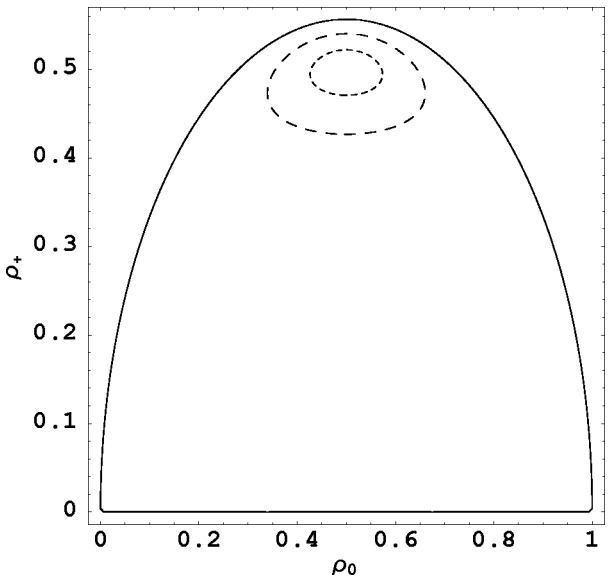


FIG. 4. Closed orbits obtained from Eq. (4.15) for $\mu=0.12$ and $\mathcal{E}=0$ (solid line), $1.7\times10^{-4}$ (dotted line), and $10^{-4}$ (dashed line).

to be *unstable*. Notice that Eq. (4.15) is invariant under the transformation $\rho_0\to1-\rho_0$. This implies that the sufficient condition for instability with respect to perturbations orthogonal to the invariant manifold $\mathcal{M}^-$ can be presented as

$$\Gamma(\rho_0,\rho_+)+\Gamma(1-\rho_0,\rho_+)>0, \tag{4.20}$$

which, upon substituting the expression for $\Gamma$ [Eq. (4.18)] takes the form

$$\rho_+^2>8\mu\rho_0(1-\rho_0). \tag{4.21}$$

The periodic orbits are unstable if the largest periodic orbit defined by Eq. (4.16) lies completely inside this instability boundary. This happens at $1+2\mu<8\mu$, i.e., $\mu>1/6$. This means that the stability boundary, if it exists, should be contained in the interval $0<\mu<1/6$. We have numerically integrated Eq. (4.13) for different values of $\mu<1/6$, and found that condition (4.19) is satisfied for $\mu<\mu_c$ where $\mu_c=1/8$. All the orbits, including the fixed point, have the same critical value of $\mu_c$. In the interval $1/6>\mu>1/8$ small-amplitude (large-energy) orbits are stable, while large-amplitude (small-energy) orbits are not. The dynamics on the $\mathcal{M}^+$ invariant manifold is less interesting. On $\mathcal{M}^+$ the dynamics is governed by

$$\begin{aligned}\dot\rho_0&=-\rho_0+\rho_0^2-\rho_-^2,\\ \dot\rho_-&=(\mu+\nu\rho_0)\rho_-.\end{aligned} \tag{4.22}$$

When both $\mu$ and $\nu$ are positive, the Turing mode $\rho_0$ relaxes to zero, whereas $\rho_-$ becomes unbounded. On the contrary, when both $\mu$ and $\nu$ are negative, $\rho_-$ relaxes to zero, whereas $\rho_0$ becomes unbounded. In the case $\mu>0$ and $\nu<0$ the manifold $\mathcal{M}^+$ is unstable to orthogonal perturbations. In the case $\mu<0$ and $\nu>0$, there is a stationary solution $\rho_0=|\mu|/\nu$ and $\rho_-=\sqrt{\rho_0(\rho_0-1)}$. Linearizing the system around this solution we find that it is always unstable. The trajectories either run away to infinity or are attracted to the trivial state $\rho_0=\rho_-=0$.

## V. CONCLUSION

The results of the above analysis turned out to be far from straightforward. It is reasonable to expect that resonant interaction between Turing modes, which are always destabilizing at a nondegenerate Turing bifurcation, would restrict the parameter region where the amplitudes remain finite in the absence of higher-order (cubic) terms. This is, indeed, confirmed by the results of Sec. IV. The stabilization by quadratic terms only remains possible in a reduced parameter domain shrinking as $\kappa$ increases, and the stability boundaries at $\kappa\ll1$ can be obtained by regular perturbation expansion. A surprising fact, however, is the appearance of another branch of stable dynamic solutions which disappears at $\kappa\leqslant\kappa_c$, and can be constructed using a *singular* perturbation technique only. Thus, the character of the finite amplitude solutions changes in a qualitative way when the Turing-mode–Turing-mode resonance is present.

## ACKNOWLEDGMENTS

The authors are grateful to A. Nepomnyashchy for helpful discussions. The work of Z.H.M. was supported by a grant from the Israeli Ministry of Science. L.M.P. acknowledges support by the Technion V.P.R. Fund.

## APPENDIX: A MODEL SYSTEM

In this Appendix we derive the required conditions for wave-mode–Turing-mode resonance to occur and compute coefficients of amplitude equations for a model system, which is much simpler than the nonlinear optical systems considered in earlier studies. Consider the following three-component reaction-diffusion system:

$$\begin{aligned}u_t&=\nabla^2u+u-u^2+v+w,\\ v_t&=\delta\nabla^2v-\gamma v-\eta u,\\ 0&=\beta\nabla^2w-\nu u-w.\end{aligned} \tag{A1}$$

Linearizing Eq. (A1) around its trivial zero solution we get the eigenvalue problem $\mathcal{L}\boldsymbol{u}=\boldsymbol{0}$, where the linear operator $\mathcal{L}$ is defined by

$$\mathcal{L}=\begin{pmatrix}\partial_t-\nabla^2-1 & -1 & -1\\ \eta & \partial_t-\delta\nabla^2+\gamma & 0\\ \nu & 0 & -\beta\nabla^2+1\end{pmatrix}.$$

Presenting the linear term $\boldsymbol{u}=(u,v,w)$ as the sum of $N$ bifurcation modes with wave vectors $\boldsymbol{q}_j(j=1,2,\ldots,N)$ and frequency $\sigma$,

$$\boldsymbol{u}=\sum_{j=1}^{N}\hat{\boldsymbol{u}}_j\exp(i\boldsymbol{q}\cdot\boldsymbol{x}+\sigma t)+\text{c.c.}, \tag{A2}$$

and substituting into the eigenvalue equation $\mathcal{L}\boldsymbol{u}=\boldsymbol{0}$, we arrive at the following dispersion relation:

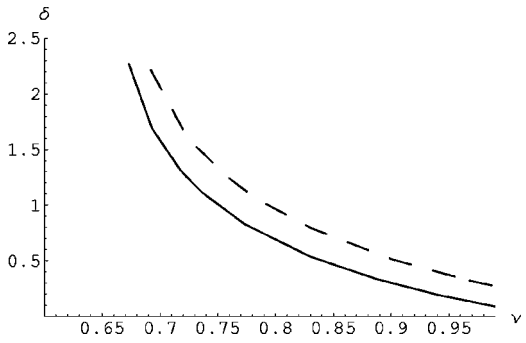


FIG. 5. Locus of the wave-mode–Turing-mode resonant bifurcation in the $(\delta,\nu)$ space for $\gamma=0.334$, and $\beta=6$ (solid line), $\beta=7$ (dashed line).

$$\sigma^2+f(q^2)\sigma+h(q^2)=0, \tag{A3}$$

where the coefficients $f(q^2)$ and $h(q^2)$ are given by

$$f(q^2)=(\delta+1)q^2+\frac{\nu}{\beta q^2+1}+\gamma-1, \tag{A4}$$

$$h(q^2)=(\delta q^2+\gamma)\left(q^2+\frac{\nu}{\beta q^2+1}-1\right)+\eta.$$

Stability of the trivial solution against zero-mode $(q=0)$ perturbations implies $\nu>1-\eta/\gamma$ and $\gamma+\nu-1>0$. However, this solution may lose stability as a result of diffusion-driven instability $(q\neq 0)$. The resulting instability may be static (Turing) or oscillatory (Hopf or wave). In the following, we are interested in the conditions when wave-mode–Turing-mode resonance occurs. The condition of Turing instability is $h(q^2)=0$, $f(q^2)>0$, and the condition of wave instability is $f(q^2)=0$, $h(q^2)>0$. The location of the wave-mode–Turing-mode resonance in the $(\delta,\nu)$ parametric space is shown in Fig. 5. A typical example of the dispersion relation in the case of wave-mode–Turing-mode resonance is shown in Fig. 6(a), as contrasted to an off-resonance dispersion relation in Fig. 6(b).

For the purpose of weakly nonlinear analysis of the system (A1), we follow the standard method of multiple-scale bifurcation expansion. We introduce a hierarchy of time scales $t_0=t, t_1=\epsilon t, \ldots$ with

$$\partial/\partial t=\partial/\partial t_0+\epsilon\partial/\partial t_1+\epsilon^2\partial/\partial t_2+\cdots, \tag{A5}$$

and expand in a power series the field variable $\boldsymbol{u}$ and the bifurcation parameters denoted as an array $\boldsymbol{p}=\{\delta,\gamma,\eta,\beta,\nu\}$:

$$\boldsymbol{u}=\epsilon\boldsymbol{u}_1+\epsilon^2\boldsymbol{u}_2+\cdots, \tag{A6}$$

$$\boldsymbol{p}=\boldsymbol{p}_0+\epsilon\boldsymbol{p}_1+\epsilon^2\boldsymbol{p}_2+\cdots. \tag{A7}$$

Using the above expansions in system (A1), we recover in the first order in $\epsilon$ the corresponding linear eigenvalue problem. In the next order we arrive at the following nonlinear inhomogeneous problem:

$$\mathcal{L}\boldsymbol{u}_2=-\mathcal{J}\boldsymbol{u}_1-u_1^2\hat{e}_1, \tag{A8}$$

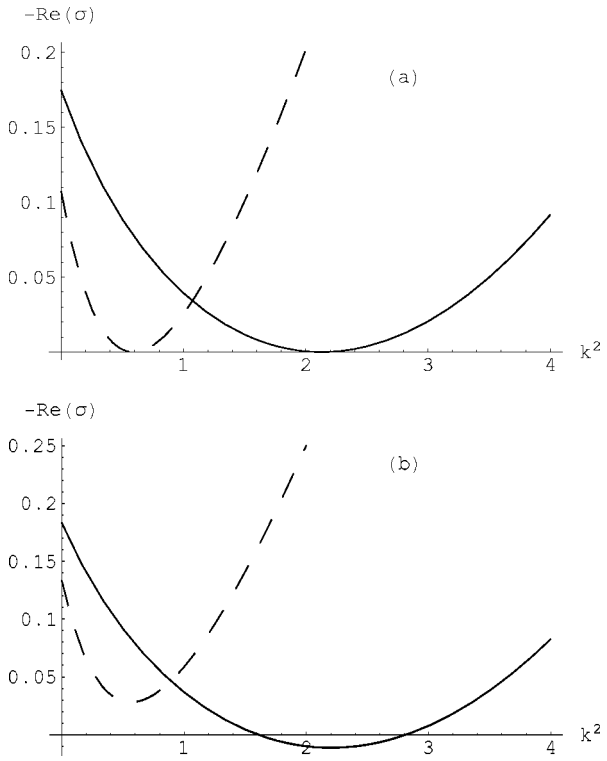


FIG. 6. Dispersion relation corresponding to Hopf (dashed line) and Turing (solid line) instabilities. The values of the parameters are (a) $\delta=0.831$, $\nu=0.774$ and (b) $\delta=0.95$, $\nu=0.8$. The other parameters are $\gamma=0.334$, $\eta=0.25$, and $\beta=6$.

where $u_1$ is the first component of $\boldsymbol{u}_1$ and $\hat{e}_1=(1,0,0)$. The linear operator $\mathcal{J}$ is defined by

$$\mathcal{J}=\begin{pmatrix}\partial_{t_1} & 0 & 0\\ \eta_1 & \partial_{t_1}-\delta_1\nabla^2+\gamma_1 & 0\\ \nu_1 & 0 & -\beta_1\nabla^2\end{pmatrix}. \tag{A9}$$

The amplitude equations are obtained as solvability conditions of Eq. (A8), i.e., conditions of the orthogonality of the inhomogeneity to all eigenfunctions of the adjoint linear problem, with respect to the scalar product defined by

$$\langle\boldsymbol{\phi}|\boldsymbol{\psi}\rangle=\sum_{j=1}^{3}\int\phi_j^*\psi_j d^2x.$$

A possible resonant structure consists of two wave modes with wave number $k$ and one Turing mode with wave number $Q$. Such a resonant structure has the form (2.2), and satisfies the resonance condition $\boldsymbol{q}-\boldsymbol{k}=\boldsymbol{Q}$. The eigenvectors of the linear eigenvalue problem are given by

$$\boldsymbol{U}_s=\left(-1,\frac{\eta}{\delta Q^2+\gamma},\frac{\nu}{\beta Q^2+1}\right), \tag{A10}$$

$$\boldsymbol{V}_w=\left(-1,\frac{\eta}{i\omega+\delta q^2+\gamma},\frac{\nu}{\beta q^2+1}\right),$$

where $\omega$ is the Hopf frequency given by

$$\omega = \sqrt{(\delta q^2+\gamma)(q^2-1)+\nu\frac{\delta q^2+\gamma}{\beta q^2+1}+\eta}. \tag{A11}$$

Projecting the right-hand side of Eq. (A8) on the eigenvectors of the adjoint linear problem given by

$$\boldsymbol{U}_s^\dagger = \left(1, \frac{1}{\delta Q^2+\gamma}, \frac{1}{\beta Q^2+1}\right),$$

$$\boldsymbol{V}_w^\dagger = \left(1, \frac{1}{-i\omega+\delta q^2+\gamma}, \frac{1}{\beta q^2+1}\right),$$

we arrive at the system of amplitude equations (2.3), where $\mu_s, \mu_w$ depend on the deviation from the bifurcation point while $\nu_s, \nu_w$, and $\lambda_s$ are computed at the bifurcation point; $\mu_s$, $\nu_s$, and $\lambda_s$ are real, while $\mu_w$ and $\nu_w$ are complex. The expressions for the coefficients are

$$\mu_s = \frac{\eta_1(\delta_0 Q^2+\gamma_0)-\eta_0(\delta_1 Q^2+\gamma_1)}{(\delta_0 Q^2+\gamma_0)^2-\eta_0} + \frac{[\nu_1(\beta_0 Q^2+1)-\nu_0\beta_1 Q^2](\delta_0 Q^2+\gamma_0)^2}{[(\delta_0 Q^2+\gamma_0)^2-\eta_0](\beta_0 Q^2+1)^2},$$

$$\mu_w = \frac{\eta_1(i\omega+\delta_0 q^2+\gamma_0)-\eta_0(\delta_1 q^2+\gamma_1)}{(i\omega+\delta_0 q^2+\gamma_0)^2-\eta_0} + \frac{[\nu_1(\beta_0 q^2+1)-\nu_0\beta_1 q^2](i\omega+\delta_0 q^2+\gamma_0)^2}{[(i\omega+\delta_0 q^2+\gamma_0)^2-\eta_0](\beta_0 q^2+1)^2},$$

$$\nu_s = \frac{2(\delta_0 Q^2+\gamma_0)^2}{(\delta_0 Q^2+\gamma_0)^2-\eta_0}, \quad \nu_w = \frac{2(i\omega+\delta_0 q^2+\gamma_0)^2}{(i\omega+\delta_0 q^2+\gamma_0)^2-\eta_0},$$

$$\lambda_s = \frac{2(\delta_0 Q^2+\gamma_0)^2}{(\delta_0 Q^2+\gamma_0)^2-\eta_0}.$$


[1] L. M. Pismen, Phys. Rev. A **23**, 334 (1981).
[2] S. Alexander and J. McTague, Phys. Rev. Lett. **41**, 702 (1978).
[3] B. A. Malomed, A. A. Nepomnyashchy, and M. I. Tribelsky, Zh. Éksp. Teor. Fiz. **96**, 684 (1989) [Sov. Phys. JETP **69**, 388 (1989)].
[4] B. Christiansen, P. Alstrom, and M. T. Levinsen, Phys. Rev. Lett. **68**, 2157 (1992).
[5] W. S. Edwards and S. Fauve, Phys. Rev. E **47**, R788 (1993).
[6] H. W. Müller, Phys. Rev. A **49**, 1273 (1994).
[7] W. Zhang and J. Vinals, Phys. Rev. E **53**, R4283 (1996).
[8] A. A. Golovin, A. A. Nepomnyashchy, and L. M. Pismen, Physica D **81**, 117 (1995).
[9] S. A. Akhmanov, M. A. Vorontsov, V. Yu. Ivanov, A. V. Larichev, and N.I. Zelenykh, J. Opt. Soc. Am. B **9**, 78 (1992).
[10] E. Pampaloni, S. Residori, and F. T. Arecchi, Europhys. Lett. **24**, 647 (1993).
[11] E. Pampaloni, P. L. Ramazza, S. Residori, and F. T. Arecchi, Phys. Rev. Lett. **74**, 258 (1995).
[12] S. Residori, P. L. Ramazza, E. Pampaloni, S. Boccaletti, and F. T. Arecchi, Phys. Rev. Lett. **76**, 1063 (1996).
[13] E. Pampaloni, S. Residori, S. Soria, and F. T. Arecchi, Phys. Rev. Lett. **78**, 1042 (1997).
[14] B. Y. Rubinstein and L. M. Pismen, Phys. Rev. A **56**, 4264 (1997).
[15] B. Y. Rubinstein and L. M. Pismen, Opt. Commun. **145**, 159 (1998).
[16] L. M. Pismen and B. Y. Rubinstein, Chaos, Solitons and Fractals **10**, 761 (1999).
[17] D. Leduc, M. Le Berre, E. Ressayre, and A. Tallet, Phys. Rev. A **52**, 1072 (1996).
[18] Yu. A. Logvin, T. Ackemann, and W. Lange, Europhys. Lett. **38**, 583 (1997).
[19] Z. H. Musslimani and L. M. Pismen, Phys. Rev. A **59**, 1571 (1999).
[20] In that case, the amplitude equations are of the gradient type, and hexagonal patterns are selected by energy minimization.
[21] Notice that the bifurcation line $\nu = 2\mu$ is not generic. Addition of higher-order terms to the amplitude equations will break the degeneracy of the Hopf bifurcation.